Available online at www.sciencedirect.com
ScienceDirect
Earth and Planetary Science Letters 256 (2007) 466–472
EPSL
www.elsevier.com/locate/epsl

Complete wetting of olivine grain boundaries by a hydrous melt near the mantle transition zone

Takashi Yoshino [a,b,*], Yu Nishihara [c,d], Shun-ichiro Karato [c]

[a] Department of Earth and Environmental Sciences, Rensselaer Polytechnic Institute, Troy, NY 12180, USA
[b] Institute for Study of the Earth's Interior, Okayama University, Misasa, Tottori 682-0193, Japan
[c] Department of Geology and Geophysics, Yale University, New Haven, CT 06511, USA
[d] Department of Earth and Planetary Sciences, Tokyo Institute of Technology, Tokyo 152-8551, Japan

Received 5 April 2006; received in revised form 23 January 2007; accepted 4 February 2007
Available online 9 February 2007
Editor: R.D. van der Hilst

Abstract

Many physical properties of liquid-bearing rocks in the deep Earth's interior are strongly controlled by its wetting behavior. We report experimental results on the variation of dihedral angle and microstructures in the forsterite–H_2O system at 1200 °C and pressures ranging from 1 to 13 GPa. The dihedral angle of the system decreases systematically with pressure and above the mantle transition zone (~ 400 km depth) it becomes approximately 0°, corresponding to completely wetted grain boundaries. This condition is probably reached because of a decrease in the solid–liquid interfacial energy with pressure due to the dramatically increased solubility of silicates in the liquid. These results suggest that the presence of partial melt would have drastic influences on physical properties of upper mantle around the transition zone even if the melt fraction is very low. Low velocity regions just above the mantle transition zone may result from the presence of hydrous melt.

Keywords: dihedral angle; grain boundary; olivine; transition zone; upper mantle; water; wetting property

1. Introduction

Pore morphology in liquid-bearing texturally equilibrated rocks significantly controls many physical properties such as elasticity, electrical conductivity and permeability of the Earth's deep materials [1–4]. The dihedral angle characterizing the geometry of the liquid phase in an olivine-rich matrix is a key factor for understanding the physical behavior of the upper mantle. In an idealized system composed of identically sized grains with isotropic interfacial energy, the dihedral angle (θ) at solid–liquid–solid triple junction is a fundamental factor in determining the connectivity of liquid and the pore morphology. It is defined by [e.g., 3,5]

$$\frac{\gamma_{ss}}{\gamma_{sl}} = 2\cos\left(\frac{\theta}{2}\right) \quad (1)$$

where γ_{ss} is the grain boundary energy per unit area and γ_{sl} is the solid–liquid interfacial energy per unit area. At low liquid volume fraction (φ), connectivity of the liquid phase is critically dependent upon θ. If $\theta < 60°$, liquid forms an interconnected network along the

* Corresponding author. Institute for Study of the Earth's Interior, Okayama University, Misasa, Tottori 682-0193, Japan.Tel.: +81 858 43 3734; fax: +81 858 43 3450.
E-mail address: tyoshino@misasa.okayama-u.ac.jp (T. Yoshino).

0012-821X/$ - see front matter © 2007 Elsevier B.V. All rights reserved.
doi:10.1016/j.epsl.2007.02.002

grain edge (triple junction) and corner (four-grain junction). If $\theta > 60°$, liquid forms isolated pockets at the grain corner or on the grain boundary, and a critical liquid fraction is necessary to establish connectivity [3,6]. Therefore, the interconnectivity of liquid phase has been evaluated by measuring dihedral angles. For the upper mantle, previous studies of wetting behavior at low pressures (<3 GPa) revealed dihedral angles of 30–50° for the basalt–olivine system [7] and 65–90° for olivine–CHO fluid system [8]. Recent studies for the olivine–H_2O system, however, suggested that the dihedral angle decreases with increasing pressure (or temperature), but the existing works are limited to ~ 5 GPa and show only a modest decrease in dihedral angle [9–11]. Mibe et al. [10] suggested that large scale transport of aqueous fluid is possible above 2 GPa, because the dihedral angle in the forsterite–H_2O system becomes less than 60° above 2 GPa. Although the critical dihedral angle for interconnection of fluid is 60°, if the smaller dihedral angle approaching 0° is established at higher pressures, many physical properties in liquid-bearing upper mantle rocks would drastically change. Therefore, further knowledge of pressure dependence of dihedral angle for the olivine–H_2O system is needed to understand anomalous properties such as low seismic velocity anomaly, seismic attenuation and electrical conductive anomaly observed in the upper mantle. In this study, we investigated a variation of dihedral angle as a function of pressure at constant temperature (1200 °C).

2. Experimental procedure

We performed high-pressure experiments to investigate the morphology of hydrous liquid in an olivine-rich matrix. A piston cylinder apparatus was used for experiments up to 3 GPa and the Kawai type multi-anvil apparatus (1000 tons) for experiments above 4 GPa. The starting material has a composition of Mg_2SiO_4+5.1 wt.% H_2O that was prepared from a mixed powder of reagent-grade Mg_2SiO_4, $Mg(OH)_2$ and SiO_2. The starting materials were once placed in a Re capsule. The Re capsule was placed in a AuPd capsule that was welded at both ends. Experiments were conducted at 1200 °C and a wide range of pressure from 1 to 13 GPa, corresponding to the field where forsterite coexists with hydrous liquid [12,13]. The samples were compressed to the desired pressure at room temperature. Then the temperature was increased to the desired temperature and kept constant within 5 °C of the desired value for a time interval between 5 and 168 h. Temperature was continuously monitored by a WRe_5–WRe_{26} thermocouple. Quenching to room temperature was achieved within a minute and pressure was then released to atmospheric pressure. After completion of an experiment, the AuPd capsule was recovered from the surrounding pressure medium (MgO). A polished section of the sample was vacuum-impregnated with epoxy to minimize plucking of grains and ground repeatedly. The final grinding step was followed by polishing using a colloidal silica. Dihedral angle measurements were made

Table 1
Summary of runs

Run no.	P (GPa)	Time (h)	θ (N) [a]	(wt.%) [b]	Mg/Si [c]	Phase [d]
FW03	1	24	46 (119)	n.d.	n.d.	Fo+OEn+L
FW09	2	72	38 (200)	n.d.	n.d.	Fo+OEn+L
FW05	3	6	34 (130)	n.d.	n.d.	Fo+OEn+L
FW01	3	24	30 (128)	n.d.	n.d.	Fo+OEn+L
FW08	3	168	31 (204)	n.d.	n.d.	Fo+OEn+L
K332	4	24	25 (162)	52 (9)	1.39 (25)	Fo+OEn+L
K331	5	48	18 (190)	46 (4)	1.85 (30)	Fo+OEn+L
K316	7	6	<10	57 (10)	1.88 (26)	Fo+OEn(+Br)+L
K315	13	5	<10	79 (11)	2.14 (16)	Fo+CEn(+Br)+L

All experiments were conducted at 1200 °C.

[a] Dihedral angle in degree determined from the median of apparent dihedral angles on the polished section. Numbers in parentheses represent numbers of analyzed angles.

[b] Weight percent of silicate component in liquid determined from electron microprobe analysis using defocused beam. The percent water in fluid is 100 minus the silicate component. Numbers in parentheses represent the standard deviation (1 sigma).

[c] Molar ratio of Mg over Si in liquid. Numbers in parentheses represent the standard deviation (1 sigma).

[d] Phases were identified using micro-Raman spectrometer and electron microprobe. Fo: forsterite, OEn: orthoenstatite, CEn: clinoenstatite, Br: brucite, L: hydrous liquid. A presence of small amounts of orthoenstatite in runs up to 5 GPa may suggest that Mg/Si molar ratio of a starting material is somewhat lower than 2. Orthoenstatite and brucite only appear at the edge of the sample (lower temperature part). Avoiding these areas, we measured dihedral angles only corresponding to the forsterite–liquid–forsterite contacting angle.

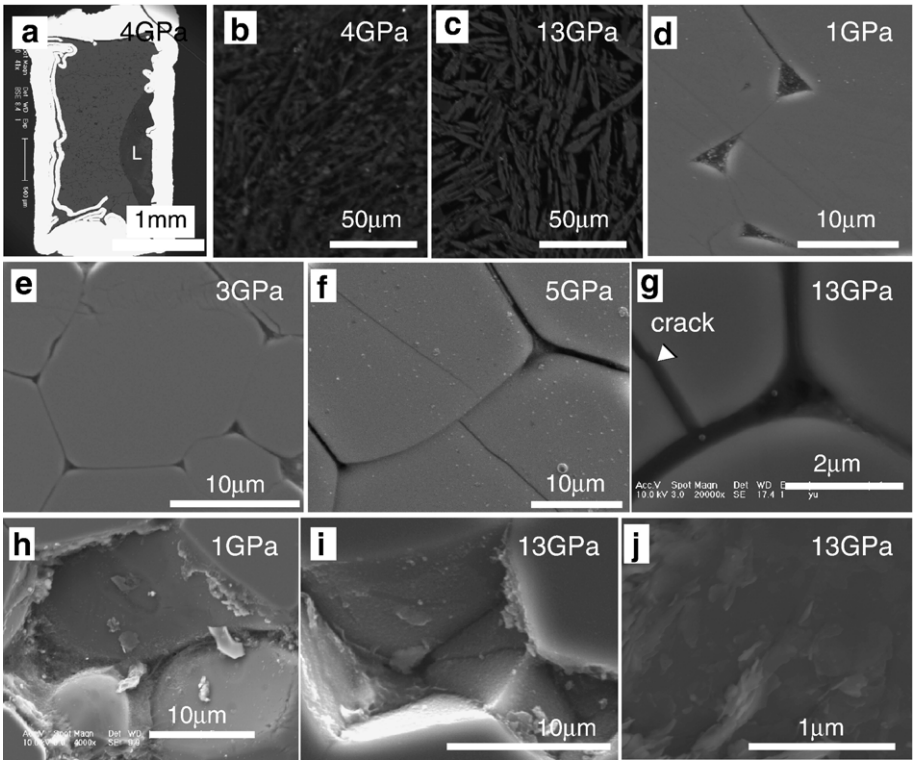

Fig. 1. Secondary-electron (SEI) and back-scattered electron (BEI) images of the forsterite + H_2O system. Fluid-filled grain junctions are now filled with epoxy or air (black area). (a) Overview BEI of the run product (Sample K332) showing liquid segregation. L represents a liquid segregation part. Note the abundant quench crystals with a columnar shape in liquid-segregated region. BEIs showing quench crystals in liquid-segregated region of (b) 4 GPa (Sample K332) and (c) 13 GPa (Sample K315). Note that the amount of quench materials increases with increasing pressure. SEIs showing pore geometries of synthetic forsterite aggregates at various pressure conditions (d) 1 GPa (Sample FW03), (e) 3 GPa (Sample FW01), (f) 5 GPa (Sample K331) and (g) 13 GPa (Sample K315). Note that separation of grain boundaries becomes common with increasing pressure. SEIs showing the presence of quench crystals (slightly bright tiny dots) on the crystal surfaces at plucking part (h) 1 GPa and (i) 13 GPa. Quench products in (h) are not common on the grain surfaces, while the surface in (i) are nearly covered with the quench material. Bright large fragments represent epoxy. (j) High-magnification view of quench materials on the grain surface from a sample (K315). Note that a shape of the quench materials is similar to that of a liquid segregation part.

from secondary-electron images at ≥2000× taken by field emission scanning electron microscope (FESEM). In a large population of over 100, measurements were carried out for each sample in the random cross section. A true dihedral angle was adopted as the median of apparent angles on the polished section, the principle of which has been reported elsewhere [14,15]. Phases including crystals quenched from liquid were identified using micro-Raman spectrometer and electron microprobe.

To determine the solubility of Mg-silicate in the hydrous liquid, we conducted two different analyses (electron microprobe and image analyses) for the runs conducted at pressure above 4 GPa, which includes a large amount of quench crystals in the segregated part. The electron microprobe analyses of the liquid phase were performed with a defocused beam (aperture of 10 or 20 μm) in order to average the chemical composition of the phases quenched from the liquid. For the image analysis, back-scattered electron images (×2000) were taken of the liquid segregated portion. The quench crystals can be recognized as a bright portion compared to the pores filled with air or epoxy in the back-scattered image. The gray-scale images were converted to binary images, and the quench crystals were separated using the threshold function of the Image J software provided by NIH. For each sample, five images were analyzed. The silicate contents in the liquid were determined from densities of forsterite [16] and H_2O [17] based on the volume fraction of quench crystals. It is unclear whether the volume ratio was established at the room condition or the run pressure condition, so we present a range of silicate component in the liquid based on these two extreme cases (Fig. 4a). For the case of the run pressure condition, the weight proportions of the Mg-silicate component were calculated using a density of ice VII [17], because ice VII is a stable form of H_2O at the room temperature under the run pressures. All quench crystals were treated as forsterite, which was confirmed by micro-

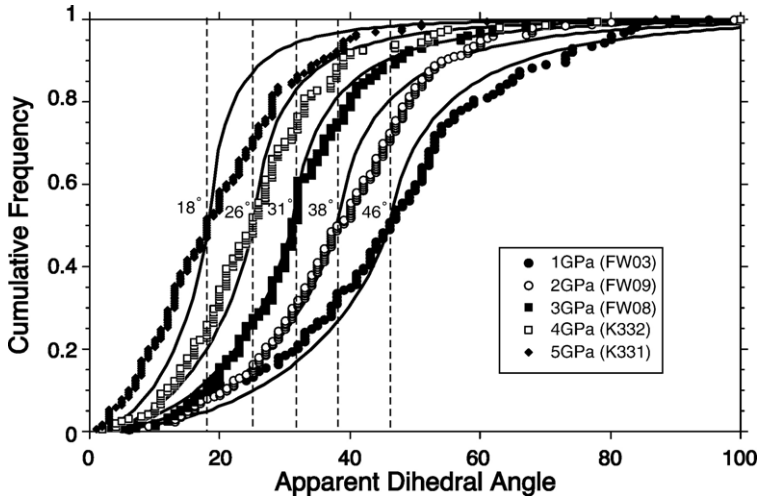

Fig. 2. Cumulative frequency distributions for apparent dihedral angles in various pressure experiments (1 to 5 GPa). The thick curves are theoretical distributions calculated assuming that the median is the true dihedral angle [14]. The dotted lines indicate the median angle determined from each run.

Raman spectroscopy as for the run products of higher-pressure experiments (>7 GPa). The possible presence of enstatite as a quench material may reduce the actual solid component in the liquid. Details of the experimental conditions and results are shown in Table 1.

3. Experimental results

3.1. Microstructure

The run products consist of forsterite and hydrous liquid with a very small amount of orthoenstatite and clinoenstatite. Above 7 GPa a quite small amount of brucite was noted at the coldest part of the capsule. Segregation of hydrous liquid due to the thermal gradient in the cell assembly was commonly observed in any sample, especially above 4 GPa (Fig. 1a). The proportion and size of quench crystals increase with increasing pressure (Fig. 1b–c). For the higher pressure runs (above 7 GPa), forsterite was identified as a quenched phase by micro-Raman spectroscopy (Fig. 1c). Chemical compositions of the liquid phase show higher total weight percentage (MgO and SiO_2) and higher Mg/Si at higher pressures. Except for the highest-pressure run (13 GPa), Mg/Si less than 2 of the liquid phase may represent a presence of enstatite as the quench product (Table 1), although we could not identify the phase other than forsterite. Concentrations of Re, Au and Pd, which were used as capsules, are below detection limit. The presence of fluid along grain edges or boundaries in forsterite aggregates can be recognized as pore filled with epoxy or air and quench products on the crystal surface. For all pressure conditions, development of crystal faces (faceting) at the pore wall is uncommon, although faceting tends to produce heterogeneous liquid distribution [18,19]. The apparent contacting angle on the polished section between forsterite and aqueous fluid varies with pressure (Fig. 1d–g). Because the grain boundaries observed from the runs above 7 GPa are mostly separated, we could not determine dihedral angle for these samples. The pore walls from the triple junction to the opened grain boundary show continuous curvature

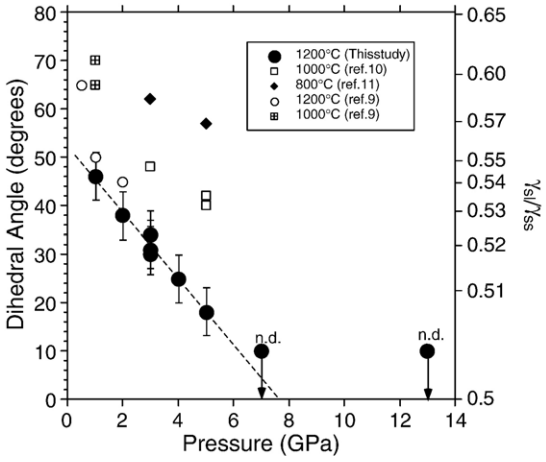

Fig. 3. Dihedral angles in the forsterite–H_2O system as a function of pressure. Analytical error is less than 5°. n.d.=not determined. It is difficult to measure dihedral angles for the samples above 7 GPa due to the grain boundary separation, but the dihedral angles expected from restricted number of measurable angles are less than 10°. Previous results of Fe-bearing olivine [9] at the same physical conditions are somewhat higher than the results of this study.

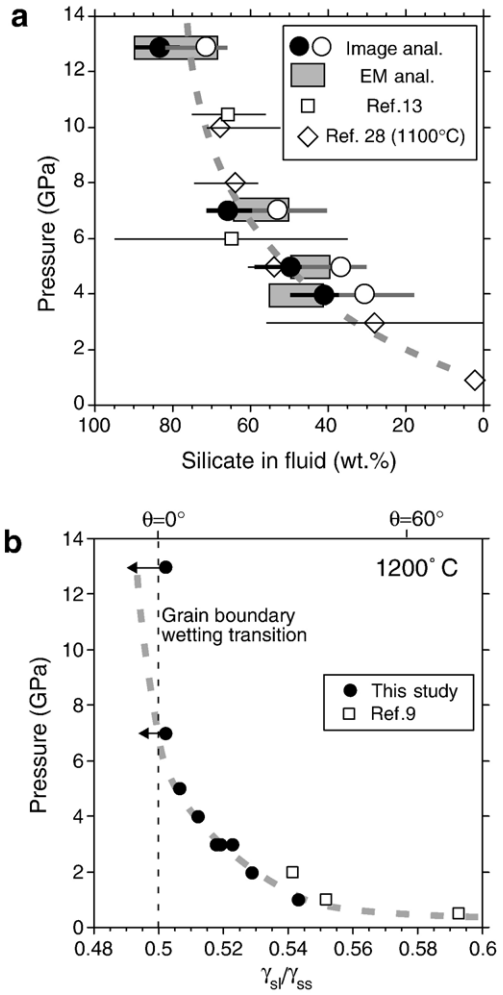

Fig. 4. Comparison between solubility of silicate components in the liquid and γ_{sl}/γ_{ss} in a wide range of pressure. (a) Weight percent of Mg-silicate component in the hydrous liquid as a function of pressure. Shaded rectangles represent the total weight percent of Mg-silicate component in the liquid determined from the electron microprobe analyses. Closed and opened circles indicate the estimated compositions from the image analyses based on densities at the room and the run pressure conditions, respectively. (b) Pressure variation of γ_{sl}/γ_{ss} under constant temperature.

without inflection points (Fig. 1g). Crystal surfaces observed in plucking areas of the samples from the lower-pressure runs are free of quench materials (Fig. 1h). At 13 GPa, however, sub-micron size quench materials with crystalline habit completely coat the crystal surfaces (Fig. 1i–j).

3.2. Dihedral angle

Time series experiments were conducted at 3 GPa for 6, 24 and 168 hour durations to investigate the effect of run duration on textural equilibration. While the mean grain sizes of forsterite increase with time, the medians of the measured angles are same within the error irrespective of run durations. Therefore, the dihedral angles determined from shorter duration experiments (~5 h) seem to be valid, since textural equilibration can be achieved as long as the distance for diffusion exceeds grain size [20].

Cumulative frequencies of apparent angles on the polished section in runs ranging from 1 to 5 GPa are shown in Fig. 2. Compared to the theoretical cumulative distribution of the median obtained from each run, the measured angles deviate significantly from the theoretical curve when apparent angles are larger than the median. This deviation may be caused by the difficulty of low angle measurements. Therefore, the true dihedral angles for samples with lower dihedral angle (<30°) are considered to be lower than the median we determined. Dihedral angles (θ) decrease from 46° to 18° with increasing pressure from 1 to 5 GPa (Fig. 3). Previous results of lower temperature experiments (800 °C and 1000 °C) [10,11] obtained from the same system show similar trends (negative $d\theta/dP$). The slope of $d\theta/dP$ at constant temperature becomes steeper with increasing temperature. If the slope is extrapolated to higher pressures, the dihedral angle becomes 0° around 7.5 GPa at 1200 °C. Above 7 GPa, it is difficult to measure the dihedral angle due to the presence of open grain boundaries, but the dihedral angles are probably lower than 10°. Open grain boundaries observed from higher pressure experiments cannot be considered as a direct evidence of a 0° dihedral angle at a higher pressure, because the grain boundaries generally dilate during decompression. However, the presence of the crystal surfaces covered with fine quench products suggests that the opening of grain boundaries during decompression is unlikely. The quench products could not move along the grain boundary and precipitate on the crystal surfaces under ambient temperature after quenching. A liquid is likely to have existed stably along the grain boundaries at the experimental condition.

4. Discussion

The present results clearly show the dependence of dihedral angle on pressure at constant temperature in the forsterite + H_2O system. The dihedral angle is expected to be small in the system in which the liquid phase has a structure and composition close to that of the solid phase [10,21–23]. In general, the solubility of the silicate component in aqueous fluid increases with increasing pressure [24–26]. On the other hand, the solubility of

water in silicate melt also increases with increasing pressure. At the second critical end point, silicate melt and aqueous fluid in the Earth's interior are expected to become indistinguishable from each other [26]. The remarkable increase in the amount of quench products at 4 GPa may represent a presence of the second critical end point between 3 and 4 GPa, and can be considered as strong evidence that the liquid composition approaches to the solid phase at higher pressure. This pressure range is similar to the second critical point for the peridotite–H_2O system (3.8 GPa and 1000 °C) [27]. The amount of dissolved Mg-silicate increases continuously up to 10 GPa at 1100 °C, where it reaches a silicate concentration in the fluid of 70 wt.% [28]. Rough estimations of dissolved Mg-silicate in the liquid show that the solid component in the liquid monotonically increases (Fig. 4a). Furthermore, the molar ratio of Mg/Si in the liquid increases with increasing pressure from 1.4 at 4 GPa to ~2 at 13 GPa (Table 1). This trend is quite consistent with previous works [12,28].

A run product recovered from 13 GPa showing the crystal surfaces covered with fine quench products can be considered as evidence of grain boundary wetting. The dihedral angle θ is defined by Eq. (1). A transition from $\theta>0°$ to $\theta=0°$ has been well known as the grain boundary wetting transition for some metallic alloy and ceramics [29]. Such a transition can occur, if some intensive thermodynamic parameter like temperature and pressure or composition is altered. In the binary system, the transition may occur at critical temperature lower than the melting point of the more refractory phase [30]. The shape of γ_{sl}/γ_{ss}–temperature (or pressure) curves generally resembles that of liquidus curves in the phase diagram [21]. Indeed, the shape of the γ_{sl}/γ_{ss}–pressure curve are quite similar to the solubility–pressure curve in the phase diagram (Fig. 4). The fact that the dihedral angles we determined from lower pressure experiments monotonically decrease toward higher pressure is consistent with the presence of the grain boundary wetting at high pressure. Therefore, we conclude that the dihedral angle of $Mg_2SiO_4+H_2O$ system becomes 0° at a certain pressure (above at least 7 GPa).

This complete wetting has drastic effects on the behavior of partial melt in the Earth's interior. First, compaction due to deformation of solids will be enhanced through fluid-phase transport (i.e., pressure–solution creep [18,31–33]). Complete wetting may slightly reduce the permeability of a bulk rock due to the change of pore shape from tube to sheet. Since the viscosity of the system, however, decreases substantially, efficiency of compaction would be largely enhanced by complete wetting. Second, if a partial melt is present under these conditions, it will dramatically reduce the seismic wave velocity and increase attenuation. The shear wave velocity drops as much as 20–30% at the 1% melt fraction [34].

In general, temperature–pressure conditions in the deep mantle are not enough to melt anhydrous peridotites [35] and hence melting under deep mantle conditions is promoted primarily by the addition of "impurities" such as water [36]. A large partitioning coefficient of water between olivine and wadsleyite ($D_{wd/ol}=5$) [37] could lead to partial melting when the upwelling materials pass the 410 km discontinuity (a top of the transition zone). Thus, if wadsleyite in the transition zone includes a certain amount of water (>0.05 wt.%), the upwelling mantle can generate hydrous melt just above the transition zone. Wetting property of the hydrous melt may be similar to that of the olivine–H_2O system at 13 GPa. Although such a partial melt would occur only under limited conditions due to the effective compaction, the total wetting of grain boundaries is possible to occur under the condition where an ultramafic melt is nearly neutrally buoyant in the upper mantle above the transition zone [38]. Recent experimental investigations of the density of hydrous melt suggested that hydrous melt with a certain amount of H_2O (<4–6 wt.%) is gravitationally stable just above the 410-km seismic discontinuity [39,40]. Low-velocity anomalies just above the 410-km discontinuity showing a shear-wave velocity drop of ~5% [41,42] might be attributed to the presence of partial melting.

Acknowledgements

The authors thank E.B. Watson for his interest, encouragement, and helpful and stimulating discussions during the course of this work. The authors are also indebted to K. Mibe, I. Katayama for discussion and P. Skemer, Z. Jiang, D. Wark for technical assistance. This work was supported by the Research Fellowships to T.Y. from the Japan Society for Promotion of Science for Young Scientists.

References

[1] H. Schmeling, Numerical models on the influence of partial melt on elastic, anelastic and electrical properties of rocks, Phys. Earth Planet. Inter. 41 (1985) 34–57.
[2] R.D. Hyndman, P.M. Shearer, Water in the lower continental crust — modeling of magnetotelluric and seismic reflection results, Geophys. J. Int. 98 (1989) 343–365.
[3] N. von Bargen, H.S. Waff, Permeabilities, interfacial areas and curvatures of partially molten systems: results of numerical

computations of equilibrium microstructures, J. Geophys. Res. 91 (1986) 9261–9276.
[4] Y. Takei, Effect of pore geometry on V_P/V_S: from equilibrium geometry to crack, J. Geophys. Res. 107 (2003) 2050, doi:10.1029/ 2001JB000522.
[5] C.S. Smith, Grains, phases and interfaces: an interpretation of microstructure, Trans. Metall. Soc. AIME 175 (1948) 15–51.
[6] T. Yoshino, M.J. Walter, T. Katsura, Core formation in planetesimals triggered by permeable flow, Nature 422 (2003) 154–157.
[7] H.S. Waff, J.R. Bulau, Equilibrium fluid distribution in an ultramafic partial melt under hydrostatic conditions, J. Geophys. Res. 84 (1979) 6109–6114.
[8] E.B. Watson, J.M. Brenan, Fluids in the lithosphere, 1. Experimentally-determined wetting characteristics of CO_2–H_2O fluids and their implications for fluid transport, host–rock physical properties, and fluid inclusion formation, Eath Planet. Sci. Lett. 85 (1987) 497–515.
[9] E.B. Watson, J.M. Brenan, D.R. Baker, in: M. Menzies (Ed.), Continental Mantle, Oxford Univ. Press, Oxford, 1991, pp. 111–125.
[10] K. Mibe, T. Fujii, A. Yasuda, Connectivity of aqueous fluid in the Earth's upper mantle, Geophys. Res. Lett. 25 (1998) 1233–1236.
[11] K. Mibe, T. Fujii, A. Yasuda, Control of the location of the volcanic front in island arcs by aqueous fluid connectivity in the mantle wedge, Nature 25 (1998) 1233–1236.
[12] T. Inoue, Effect of water on melting phase relations and melt composition in the Mg_2SiO_4–$MgSiO_3$–H_2O system up to 15 GPa, Phys. Earth Planet. Inter. 85 (1994) 237–263.
[13] R. Stalder, P. Ulmer, A.B. Thompson, D. Günther, High pressure fluids in the system MgO–SiO_2–H_2O under upper mantle conditions, Contrib. Mineral. Petrol. 140 (2001) 607–618.
[14] O.K. Riegger, L.H. van Vlack, Dihedral angle measurement, Trans. Metall. Soc. AIME 218 (1960) 933–935.
[15] S.R. Jurewicz, A.J.G. Jurewicz, Distribution of apparent angles on random sections with emphasis on dihedral angle measurements, J. Geophys. Res. 91 (1986) 9277–9282.
[16] L. Zhang, Single crystal hydrostatic compression of (Mg,Mn,Fe,Co)$_2SiO_4$ olivines, Phys. Chem. Miner. 25 (1998) 308–312.
[17] E. Wolanin, Ph. Pruzan, J.C. Chervin, B. Canny, M. Gauthier, Equation of state of ice VII up to 106 GPa, Phys. Rev., B 56 (1997) 5781–5785.
[18] U.H. Faul, D.R. Toomey, H.S. Waff, Intergranular basaltic melt is distributed in thin, elongated inclusions, Geophys. Res. Lett. 21 (1994) 29–32.
[19] T. Yoshino, J.D. Price, D.A. Wark, E.B. Watson, Effect of faceting on pore geometry in texturally equilibrated rocks: implications for low permeability at low porosity, Contrib. Mineral. Petrol. 152 (2006) 169–186.
[20] R.F. Cooper, D.L. Kohlstedt, Solution-precipitation enhanced diffusional creep of partially molten olivine–basalt aggregates during hot-pressing, Tectonophysics 107 (1984) 207–233.
[21] M. Holness, Temperature and pressure dependence of quartz–aqueous fluid dihedral angles: the control of absorbed H_2O on the permeability of quartzites, Eath Planet. Sci. Lett. 117 (1993) 363–377.
[22] T. Yoshino, K. Mibe, A. Yasuda, T. Fujii, Wetting properties of anorthite aggregates: implications for fluid connectivity in continental lower crust, J. Geophys. Res. 107 (2002), doi:10.1029/2001JB000440.
[23] Y. Takei, I. Shimizu, The effects of liquid composition, temperature, and pressure on the equilibrium dihedral angles of binary solid–liquid systems inferred from a lattice-like model, Phys. Earth Planet. Inter. 139 (2003) 225–242.
[24] G.C. Kennedy, G.J. Wasserburg, H.C. Heard, R.C. Newton, The upper three-phase region in the system SiO_2–H_2O, Am. J. Sci. 260 (1962) 501–521.
[25] C.E. Manning, The solubility of quartz in H_2O in the lower crust and upper mantle, Geochim. Cosmochim. Acta 58 (1994) 4831–4839.
[26] P.J. Wyllie, O.F. Tuttle, Experimental investigation of silicate systems containing two volatile components, Part 1. Geochemical considerations, Am. J. Sci. 258 (1960) 498–517.
[27] K. Mibe, M. Kanzaki, T. Kawamoto, K. Matsukage, Y. Fei, S. Ono, Second critical endpoint in the peridotite-H_2O system, J. Geophys. Res., (in press).
[28] K. Mibe, T. Fujii, A. Yasuda, Composition of aqueous fluid coexisting with mantle minerals at high pressure and its bearing on the differentiation of the Earth's mantle, Geochim. Cosmochim. Acta 66 (2002) 2273–2285.
[29] B. Straumal, B. Baretzsky, Grain boundary phase transitions and their influence on properties of polycrystals, Interface Sci. 12 (2004) 147–155.
[30] J.W. Cahn, Critical-point wetting, J. Chem. Phys. 66 (1977) 3667–3672.
[31] R.F. Copper, D.L. Kohlstedt, Rheology and structure of olivine–basalt partial melts, J. Geophys. Res. 91 (1986) 9315–9323.
[32] G.M. Pharr, M.F. Ashby, On creep enhanced by a liquid phase, Acta Metall. 31 (1983) 129–138.
[33] R. Raj, M.F. Ashby, On grain boundary sliding and diffusion creep, Metall. Trans. 2 (1971) 1113–1127.
[34] R.L. Stocker, R.B. Gordon, Velocity and internal friction in partial melts, J. Geophys. Res. 80 (1975) 4828–4836.
[35] E. Takahashi, I. Kushiro, Melting of a dry peridotite at high pressures and basalt magma genesis, Am. Mineral. 68 (1983) 859–879.
[36] K. Litasov, E. Ohtani, Phase relations and melt compositions in CMAS–pyrolite–H_2O system up to 25 GPa, Phys. Earth Planet. Inter. 134 (2002) 105–127.
[37] J.H. Chen, T. Inoue, H. Yurimoto, D.J. Weidner, Effect of water on olivine–wadsleyite phase boundary in the (Mg,Fe)$_2SiO_4$ system, Geophys. Res. Lett., 29 (18) (2002) 1875, doi:10.1029/2001GL014429.
[38] C.B. Agee, D. Walker, Olivine flotation in mantle melt, Earth Planet. Sci. Lett. 114 (1993) 315–324.
[39] K.N. Matsukage, Z. Jing, S. Karato, Density of hydrous silicate melt at the conditions of Earth's deep upper mantle, Nature 438 (2005) 488–491.
[40] T. Sakamaki, A. Suzuki, E. Ohtani, Stability of hydrous melt at the base of the Earth's upper mantle, Nature 439 (2006) 192–194.
[41] J. Revenaugh, S.A. Sipkin, Seismic evidence for silicate melt atop the 410 km mantle discontinuity, Nature 369 (1994) 474–476.
[42] T.R.A. Song, D.V. Helmberger, S.P. Grand, Low-velocity zone atop the 410-km seismic discontinuity in the northwestern United States, Nature 427 (2004) 530–533.